

Structural and mechanical characteristics of sphere packings near the jamming transition: From fully amorphous to quasi-ordered structures

Hideyuki Mizuno,¹ Kuniyasu Saitoh,² and Leonardo E. Silbert³

¹*Graduate School of Arts and Sciences, The University of Tokyo, Tokyo 153-8902, Japan*

²*Department of Physics, Faculty of Science, Kyoto Sangyo University, Kyoto 603-8555, Japan*

³*School of Math, Science, and Engineering, Central New Mexico Community College, Albuquerque, New Mexico 87106, USA*

(Dated: August 25, 2020)

Mechanically stable sphere packings are generated in three-dimensional space using the discrete element method, which span a wide range in structural order, ranging from fully amorphous to quasi-ordered structures, as characterized by the bond orientational order parameter. As the packing pressure, p , varies from the marginally rigid limit at the jamming transition ($p \approx 0$) to that of more robust systems ($p \gg 0$), the coordination number, z , follows a familiar scaling relation with pressure, namely, $\Delta z = z - z_c \sim p^{1/2}$, where $z_c = 2d = 6$ ($d = 3$ is the spatial dimension). While it has previously been noted that Δz does indeed remain the control parameter for determining the packing properties, here we show how the packing structure plays an influential role on the mechanical properties of the packings. Specifically, we find that the elastic (bulk K and shear G) moduli, generically referred to as M , become functions of both Δz and the structure, to the extent that $M - M_c \sim \Delta z$. Here, M_c are values of the elastic moduli at the jamming transition, which depend on the structure of the packings. In particular, the zero shear modulus, $G_c = 0$, is a special feature of fully amorphous packings, whereas more ordered packings take larger, positive values, $G_c > 0$.

I. INTRODUCTION

Many previous studies (e.g., [1–4]) have established peculiar mechanical and vibrational properties of *disordered* particulate systems close to the jamming transition. The elastic (bulk K and shear G) moduli, generically referred to as M , follow power-law scalings with the packing pressure p , and in particular, the shear modulus continuously vanishes when approach the transition, as $G \sim p^{1/2}$. Additionally, the vibrational density of states (vDOS) exhibits a characteristic plateau above the frequency ω^* , which goes to zero, following a power-law scaling of $\omega^* \sim p^{1/2}$. These critical behaviors of M and ω^* can be explained by “isostaticity”, where the excess contact number $\Delta z = z - z_c$ ($z_c = 2d$ is an isostatic number and d is the spatial dimension) is a central parameter for controlling the material properties [5–9]. Both the shear modulus G and the frequency ω^* are linearly scaled by $\Delta z \sim p^{1/2}$, i.e., $G \sim \Delta z$ and $\omega^* \sim \Delta z$. Interestingly, the same scaling laws were also found in dimer packings [10–12].

Similar to disordered systems, even *ordered* particulate systems are shown to exhibit critical scaling laws near the jamming transition [13–18]. A seminal work [13] systematically modified the structure of the system by introducing “disorder” and studied the effects of structural modifications on the distributions of the contact number and contact force. More recently, Goodrich *et al.* [14] demonstrated that although *perfectly* ordered crystals never show any critical behavior, only a small amount of disorder is enough to make the system behave as a highly disordered systems. In addition, Tong *et al.* [15] modified the structure by introducing a polydispersity η and controlling η and established a phase diagram in the packing pressure (p) and the polydispersity (η) plane

that identifies three phases, i.e., the crystal, disordered crystal, and amorphous phases. They demonstrated that even disordered crystals, which maintain an ordered lattice structure, show critical scaling behaviors near the jamming. Most recently, Tsekenis *et al.* [16, 17] showed that such disordered crystals exhibit a power-law scaling in force and gap distributions and a plateau in the vDOS, as do fully amorphous systems. Finally, using a model of perceptron [19], Ikeda [18] theoretically demonstrated that even weakly disordered crystals show jamming scaling laws. Therefore, it is now established that even ordered (but not *perfectly* ordered) systems behave as highly disordered systems near the jamming transition.

However, in this paper, we will demonstrate that structural properties also play an important role in determining the material properties of the systems. We analyze jammed particulate systems composed of monodisperse, frictionless, Hookean particles. We prepare a wide range of structures, ranging from fully amorphous to quasi-ordered structures, which are distinguished by the orientational order parameter, $Q_6 = 0.0$ (disordered) to 0.5 (ordered) [20]. For $Q_6 = 0.0$, the system is highly disordered, whereas the crystalline-like, ordered, lattice structure is observed for $Q_6 = 0.5$ (see Fig. 1). In this situation, the material properties of the systems generally depend on the packing pressure p as well as the structure Q_6 . We observe that the excess contact number Δz is always scaled as $\Delta z \sim p^{1/2}$, regardless of the value of Q_6 . Our main result is that the elastic moduli, $M = K$ (bulk modulus) and G (shear modulus), are described as functions of Δz and Q_6 :

$$M(\Delta z, Q_6) = M_c(Q_6) + \alpha_M \Delta z, \quad (1)$$

where $M_c = K_c, G_c$ are critical values at the jamming

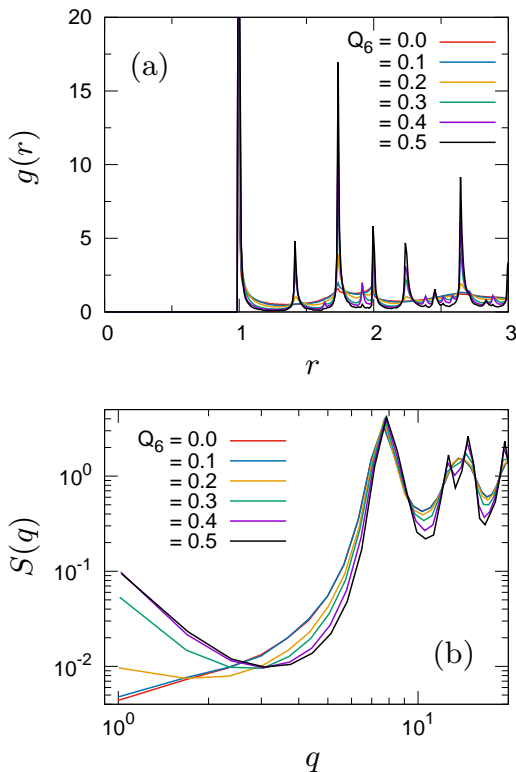


FIG. 1. Static structures in sphere packings for different values of Q_6 . The packing pressure is $p = 4 \times 10^{-6}$. We present the radial distribution function $g(r)$ in (a) and the static structure factor $S(q)$ in (b).

transition, and $\alpha_M = \alpha_K, \alpha_G$ are constants. Therefore, $M - M_c \sim \Delta z$ is controlled by Δz only and shows the same critical scaling regardless of the structure Q_6 . However, structural effects appear in M_c at the transition, and a shear modulus that is equal to zero $G_c = 0$ is a special feature of disordered packings [21–24]. For quasi-ordered packings, the shear modulus becomes finite and positive, $G_c > 0$. We will also show that this difference in G_c is reflected in the vibrational states of the systems.

II. SIMULATION MODEL

A. System preparation

Our system is composed of $N = 1,000$, monodisperse, frictionless particles with a mass m and diameter σ in three ($d = 3$) dimensional space under periodic boundary conditions. The particles interact via a finite-range, purely repulsive, harmonic potential, which has been employed in many previous simulations (e.g., [1–4]):

$$\phi(r) = \begin{cases} \frac{k}{2}(\sigma - r)^2 & (r < \sigma), \\ 0 & (r \geq \sigma), \end{cases} \quad (2)$$

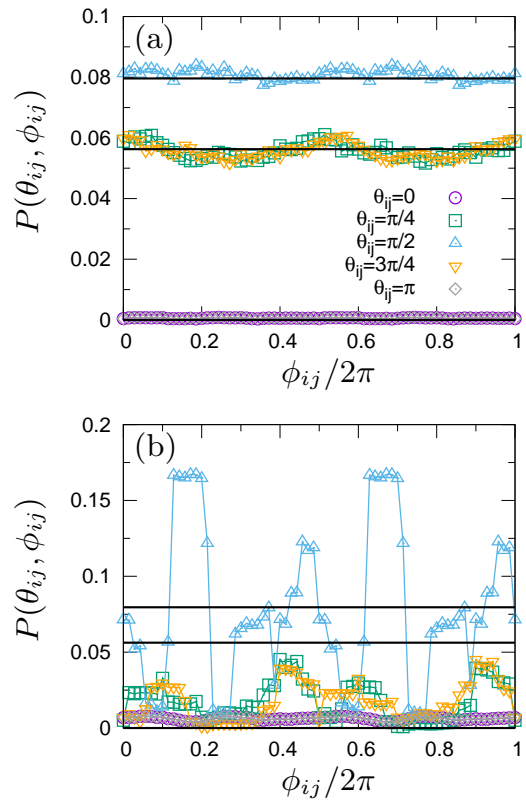


FIG. 2. Probability distribution function $P(\theta_{ij}, \phi_{ij})$ of the orientation angles of the unit bond vector $\mathbf{n}_{ij} = (\cos \phi_{ij} \sin \theta_{ij}, \sin \phi_{ij} \sin \theta_{ij}, \cos \theta_{ij})$ for $Q_6 = 0.0$ in (a) and $Q_6 = 0.5$ in (b). Note $0 \leq \phi_{ij} < 2\pi$ and $0 \leq \theta_{ij} \leq \pi$. The packing pressure is $p = 4 \times 10^{-6}$. The solid lines demonstrate the random, isotropic distribution, which coincides well with $P(\theta_{ij}, \phi_{ij})$ for the $Q = 0.0$ (disordered) case.

where r is the distance between two particles, and k parameterizes the particle stiffness and sets an energy scale through $\epsilon = k\sigma^2$. Throughout this paper, we use σ , m , and $\tau = (m/k)^{1/2}$ as units of length, mass, and time, respectively, i.e., we set $\sigma = m = k = \tau = \epsilon = 1$.

We prepare sphere packings with different structures, which are characterized by the orientational order parameter, $Q_6 = 0.0$ (disordered) to 0.5 (ordered) [20]. Here, we use a thermal decompression protocol, which has been employed as “Protocol 1” in Ref. [25]. Briefly, we prepared equilibrated liquid configurations at a temperature of $T = 10^{-3}$ and then quenched them to a very low temperature, $T = 10^{-16}$, by changing the cooling rate. The slower rate creates more ordered configurations (the larger Q_6), whereas the faster rate leads to disordered packings (the smaller Q_6).

These packings are then put into the “packing finder” (compression/decompression routine) [1] and brought to the jamming transition point (where the pressure is $p \approx 10^{-8}$). Finally, we generate the final configurations at several different packing pressures p by compressing the systems from the jamming transition. Note that we always remove the rattler particles that have fewer than

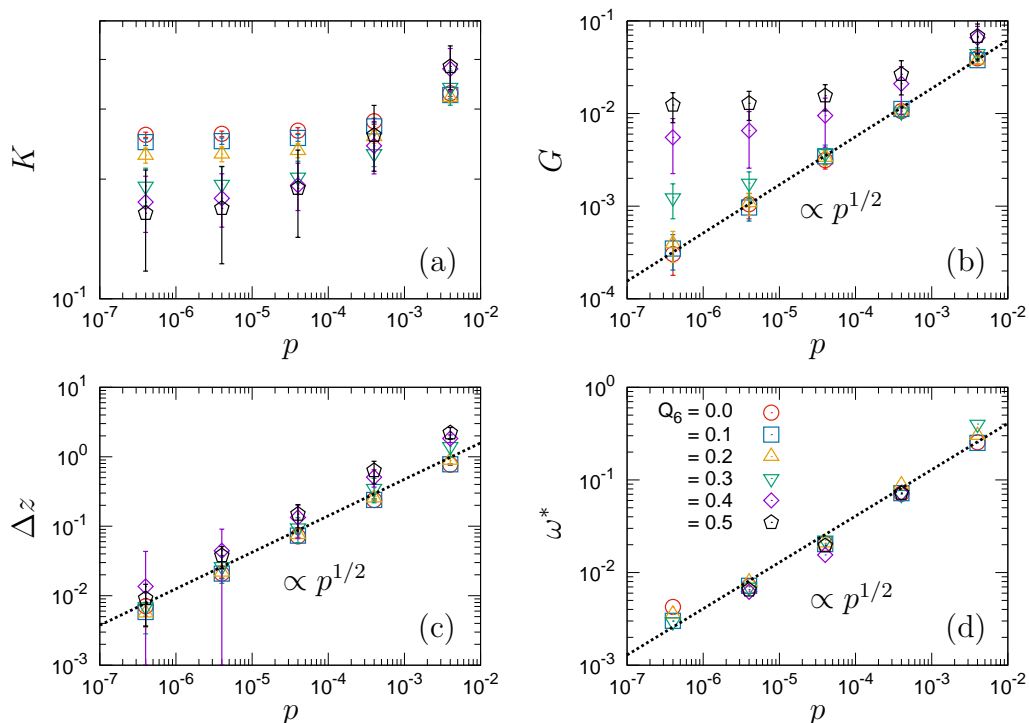


FIG. 3. Dependences on the packing pressure p of the quantities for different Q_6 values. We plot the (a) bulk modulus K , (b) shear modulus G , (c) excess contact number $\Delta z = z - z_c$, and (d) characteristic frequency in vDOS, ω^* , as functions of p . The lines represent power-law scalings with respect to p . The error bars in (a)-(c) are calculated from 100 configuration realizations.

$d = 3$ contacting neighbors. A total of 100 configuration realizations are prepared at each p and each Q_6 , and the values of the physical quantities presented below (e.g., the elastic moduli M) are obtained by taking the average of these 100 realizations.

B. Structural characteristics

Figure 1 presents the radial distribution function $g(r)$ in (a) and the static structure factor $S(q)$ in (b) for different Q_6 values and a pressure of $p = 4 \times 10^{-6}$. In the case of $Q_6 = 0.0$, we see a highly disordered structure [26]. However, as Q_6 increases toward 0.5, the system becomes a more ordered state. Indeed, we can clearly observe sharp peaks in $g(r)$, which is a feature of the crystalline-like, ordered, lattice structure. Additionally, $S(q)$ shows clear enhancement of the long-range spatial correlation at small wavenumbers q .

In addition, Figure 2 shows the probability distribution of the unit bond vector \mathbf{n}_{ij} of connected particles i and j . Here, we define the bond vector as $\mathbf{n}_{ij} = (n_{ij}^x, n_{ij}^y, n_{ij}^z) = (\cos \phi_{ij} \sin \theta_{ij}, \sin \phi_{ij} \sin \theta_{ij}, \cos \theta_{ij})$ and show the joint probability distribution $P(\theta_{ij}, \phi_{ij})$ (see Ref. [23] for details). For the case of $Q_6 = 0.0$ in (a), we clearly observe a random, isotropic distribution, $P(\theta_{ij}, \phi_{ij}) = (1/2\pi)(\sin \theta_{ij}/2)$ [21–24]. In contrast, for the ordered case of $Q = 0.5$ in (b), the distribution is completely different from this isotropic distribution.

The pronounced values in $P(\theta_{ij}, \phi_{ij})$ imply ordered structures, which is consistent with the indication of Q_6 .

III. RESULTS

In the present work, we study the mechanical and vibrational properties of disordered ($Q_6 = 0.0$) to ordered ($Q_6 = 0.5$) systems and clarify their dependences on the Q_6 value. The elastic moduli, the bulk K and shear G moduli, are calculated by using the harmonic formulation [27]. In this formulation, we can calculate elastic moduli without applying any explicit deformation field (details are found in Ref. [23]). Additionally, we diagonalize the Hessian matrix to obtain vibrational eigenmodes and calculate the vDOS, $g(\omega)$ and its characteristic frequency ω^* . Figure 3 plots the elastic moduli, K , G , excess contact number, $\Delta z = z - z_c$, and frequency, ω^* , as functions of the packing pressure p , for different Q_6 values.

A. Excess contact number Δz

We first look at the contact number and find that it takes the value of $z_c = 2d(1 - N^{-1}) \approx 6.0$ at the transition, regardless of the structural properties (Q_6). Then, the excess contact number, $\Delta z = z - z_c$, follows the same power-law scaling trend, $\Delta z \sim p^{1/2}$, for all of

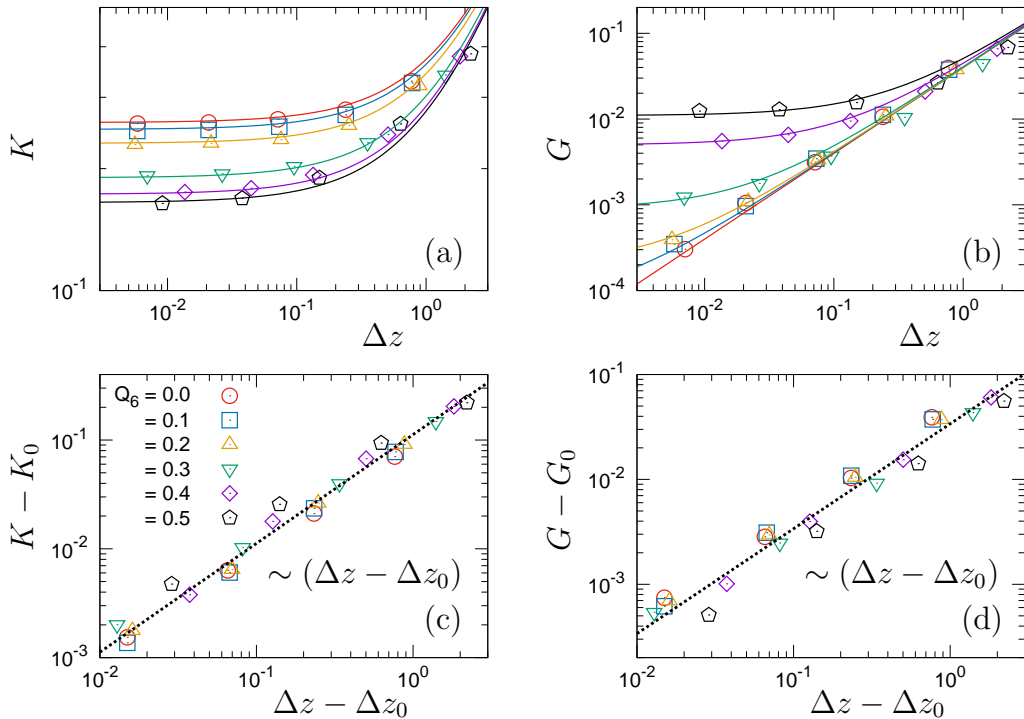


FIG. 4. Dependences on the excess contact number Δz of the elastic moduli K and G for different Q_6 values. We plot the (a) bulk modulus K and (b) shear modulus G as functions of Δz . In (c) and (d), we plot $K - K_0$ and $G - G_0$ as functions of $\Delta z - \Delta z_0$, where the subscript “0” denotes values at the lowest pressure $p = 4 \times 10^{-7}$. The data and symbols are the same as those in Fig. 3. The lines represent $K = K_c + \alpha_K \Delta z$ in (a), $G = G_c + \alpha_G \Delta z$ in (b), $K - K_0 = \alpha_K (\Delta z - \Delta z_0)$ in (c) and $G - G_0 = \alpha_G (\Delta z - \Delta z_0)$ in (d). Here, $\alpha_K \simeq 0.11$ and $\alpha_G \simeq 0.04$, and the critical values of K_c and G_c are plotted as functions of Q_6 in Fig. 5.

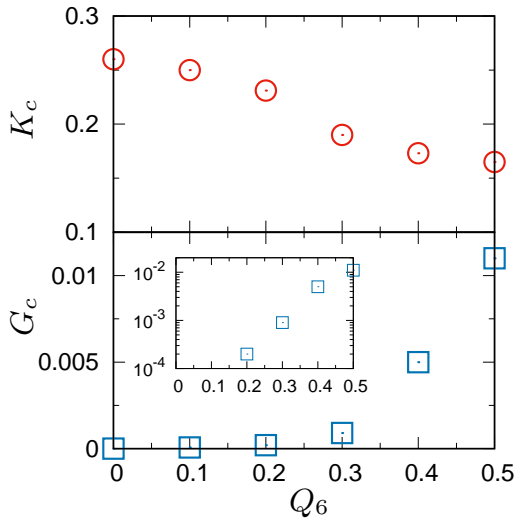


FIG. 5. Dependences on the structure Q_6 of the critical values of the elastic moduli K_c (upper panel) and G_c (lower panel). The inset to the lower panel plots G_c on the log scale.

the studied Q_6 values (see Fig. 3(c)). We note that *perfectly* ordered crystals *cannot* show such critical behavior. However, quasi-ordered systems, which are not perfectly ordered but exhibit crystalline lattice structures, as

shown in Fig. 1, can show the scaling law of $\Delta z \sim p^{1/2}$. This observation is consistent with previous simulation results [14, 15]. Ref. [14] found that only a small amount of disorder makes the system behave as a highly disordered system to exhibit the jamming scaling law. Additionally, Ref. [15] demonstrated that for the case in which polydispersity produces spatial fluctuations in the distribution of the contact number, even the system with ordered lattice structure shows critical scaling.

B. Elastic moduli $M = K, G$

In Figs. 3(a) and (b), we clearly observe that the elastic moduli K and G depend on the structural properties Q_6 . Particularly, when approaching the jamming transition as $p \rightarrow 0$, the shear modulus G vanishes continuously, following $G \sim p^{1/2}$, in a fully amorphous state of $Q_6 = 0.0$, whereas it converges to a finite value for the ordered cases with $Q_6 > 0$. We also plot K and G as functions of Δz instead of p , in Figs. 4(a) and (b) (symbols). As validated below, we can describe K and G as functions of Δz and Q_6 [Eq. (1)]:

$$\begin{aligned} K(\Delta z, Q_6) &= K_c(Q_6) + \alpha_K \Delta z, \\ G(\Delta z, Q_6) &= G_c(Q_6) + \alpha_G \Delta z, \end{aligned} \quad (3)$$

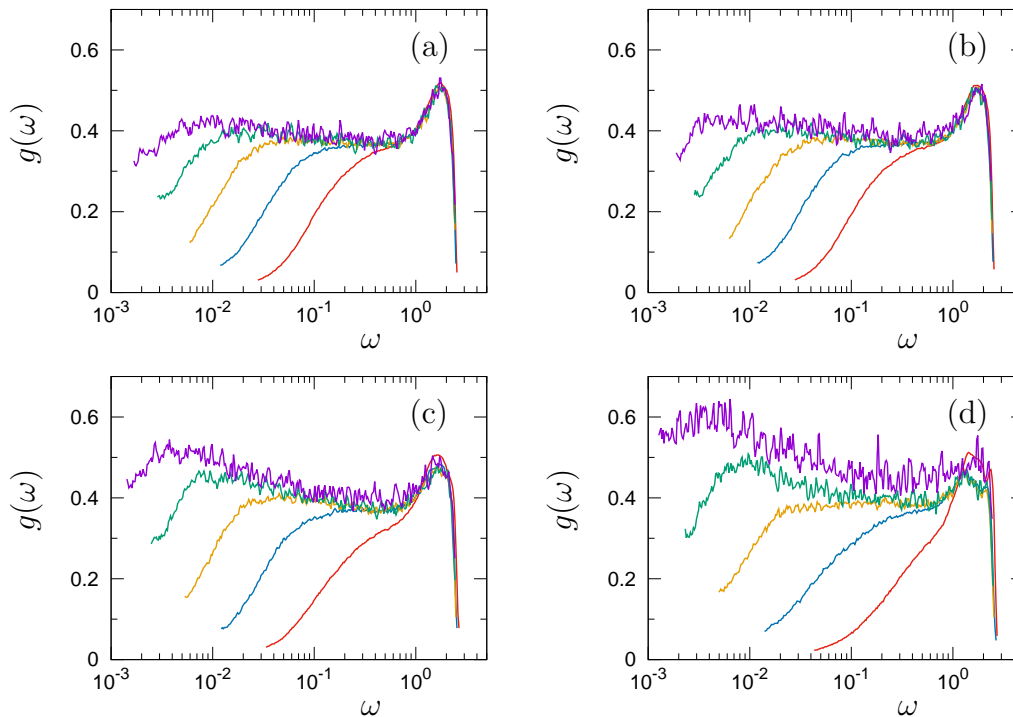


FIG. 6. The vDOS for different Q_6 values. We plot $g(\omega)$ as a function of the frequency ω for $Q_6 = 0.0$ in (a), 0.1 in (b), 0.3 in (c), and 0.5 in (d). Lines of different colors represent different packing pressures, $p = 4 \times 10^{-3}$ (red), 4×10^{-4} (blue), 4×10^{-5} (orange), 4×10^{-6} (green), and 4×10^{-7} (purple), from right to left.

where $\alpha_K \simeq 0.11$ and $\alpha_G \simeq 0.04$ are constants.

To validate Eq. (3), Fig. 4 plots $K - K_0$ in (c) and $G - G_0$ in (d) as functions of $\Delta z - \Delta z_0$, where the subscript “0” denotes values at the lowest pressure, $p = 4 \times 10^{-7}$. Both $K - K_0$ and $G - G_0$ conveniently collapse on a single curve as a function of $\Delta z - \Delta z_0$ for different Q_6 values:

$$\begin{aligned} K - K_0 &= \alpha_K (\Delta z - \Delta z_0), \\ G - G_0 &= \alpha_G (\Delta z - \Delta z_0), \end{aligned} \quad (4)$$

which determine the values of $\alpha_K \simeq 0.11$ and $\alpha_G \simeq 0.04$. In Figs. 4(a) and (b) (lines), we also plot Eq. (3) to the numerical data of K and G by using fixed values of $\alpha_K \simeq 0.11$ and $\alpha_G \simeq 0.04$ and adjusting the values of K_c and G_c . Eq. (3) (lines) fits well to the numerical data (symbols) for all the Q_6 cases, where K_c and G_c are determined as functions of Q_6 , as plotted in Fig. 5. These results validate Eq. (3) for the elastic moduli K and G .

Eq. (3) separates the dependences of K, G on the excess contact number Δz from those on the structure Q_6 . Interestingly, the scaling behaviors of $K - K_c$ and $G - G_c$ are both only controlled by Δz , regardless of Q_6 . This result indicates that the isostaticity [5–9] controls the mechanical properties near the jamming transition, regardless of whether the systems are disordered or ordered systems. However, structural effects emerge for critical values of K_c and G_c at the transition.

Figure 5 plots K_c and G_c as functions of Q_6 . The bulk modulus K_c decreases as Q_6 increases from $Q_6 = 0.0$

(disordered) to 0.5 (ordered). In contrast, the shear modulus G_c increases with increasing Q_6 . These tendencies of a more ordered system with a smaller bulk modulus and larger shear modulus are also observed in atomic glasses [28]. The zero critical value of $G_c = 0$ is a particular feature of fully amorphous packings ($Q_6 = 0.0$), which is based on the random and isotropic distribution of the bond vectors between the particles in contact (see Figs. 2(a)). A detailed discussion on this point is given in our previous work [23]. In contrast, for quasi-ordered packings, the bond distribution is neither random nor isotropic (see Figs. 2(b)), which produces the finite value of $G_c > 0$.

C. Vibrational eigenmodes

Next, the vDOSs are studied for different structures Q_6 . Figure 6 shows the $g(\omega)$ for different values of $Q_6 = 0.0$ to 0.5. In previous simulations [1, 2], the vDOS has been studied in the case of $Q_6 = 0.0$ (disordered packings). As shown in Fig. 6(a), $g(\omega)$ shows the characteristic plateau, where the vibrational eigenmodes show floppy-like motions [4]. The onset frequency of the plateau, ω^* , is controlled by the excess contact number Δz [5–9]. Upon approaching the transition, ω^* vanishes, following the power-law scaling of $\omega^* \sim \Delta z$.

Here, we can recognize the plateau even in ordered packings up to $Q_6 = 0.5$, as shown in Figs. 6(b)-(d).

Most of the recent simulations also showed a plateau in polydisperse crystalline systems [16, 17]. We note that the plateau in $g(\omega)$ is enhanced for order packings, as discussed below, but the characteristic frequency, ω^* , can still be defined for all the cases of $Q_6 = 0.0$ to 0.5 . Figure 3(d) plots ω^* as a function of p and demonstrates $\omega^* \sim p^{1/2}$ and thus $\omega^* \sim \Delta z$ for all Q_6 cases.

One noteworthy point is that the plateau in $g(\omega)$ is enhanced as the system becomes more ordered with larger Q_6 values. As demonstrated in Figs. 3 to 5, the shear modulus G_c becomes finite, *not* vanishing, in ordered packings. This finite shear modulus excites some amount of transverse acoustic modes at low frequencies, which enhances the plateau value of $g(\omega)$. Therefore, for ordered packings, acoustic modes controlled by the shear modulus G add to the floppy-like modes controlled by the excess contact number Δz , whereas for disordered packings, the acoustic modes vanish and the floppy-like modes are dominant.

IV. CONCLUSION

In summary, we have studied particulate systems near the jamming transition by varying their structural properties from fully amorphous to quasi-ordered structures. We found that “excess” elastic moduli, $\Delta M = M - M_c$ ($M = K, G$), follow the scaling law of $\Delta M \sim \Delta z$, regardless of whether there are ordered or disordered structures. However, the critical values of M_c at the transition depend on the structure. As the system becomes more ordered, the bulk modulus K_c decreases while the shear modulus G_c increases. In particular, the zero shear modulus $G_c = 0$ is the nature of fully amorphous packings, while ordered packings have a positive shear modulus of $G_c > 0$. A characteristic plateau in the vDOS and the onset frequency following $\omega^* \sim \Delta z$ are observed, which are

again common between disordered and ordered systems. However, for ordered packings, the finite shear modulus $G_c > 0$ induces transverse acoustic modes which add to the floppy-like modes controlled by Δz and enhance the plateau in the vDOS.

Our results demonstrate that the scaling laws of the mechanical and vibrational properties, which are controlled by Δz , are independent of the structural properties. This is consistent with the theoretical predictions of Refs. [5–9], which do not assume a specific structure type. However, what we found here is that critical values of K_c and G_c are controlled by the structural properties. The shear modulus only vanishes at the transition for disordered packing but not for ordered packings.

The present work and previous studies [13–18] have established that quasi-ordered systems can behave as highly disordered systems. It would be interesting to investigate how quasi-ordered systems share the material properties of disordered systems. For example, recent studies [29–32] unveiled the existence of localized vibrational modes in disordered systems and their vDOS following $g(\omega) \sim \omega^4$. In particular, it was found that the localized modes are controlled by the excess contact number near the jamming transition [5, 6, 9, 33]. Another anomalous property could be the elastic response [34–36], sound attenuation [37–42], and anharmonic (nonlinear) properties, including thermal activation [43–45], contact change [46–48], and plastic events [49–53]. We may expect that quasi-ordered systems share many of these properties and phenomena, which could be addressed in the future.

ACKNOWLEDGMENTS

This work was supported by JSPS KAKENHI Grant Numbers 18K13464, 19K14670, and 20H01868.

-
- [1] C. S. O’Hern, L. E. Silbert, A. J. Liu, and S. R. Nagel, Phys. Rev. E **68**, 011306 (2003).
 - [2] L. E. Silbert, A. J. Liu, and S. R. Nagel, Phys. Rev. Lett. **95**, 098301 (2005).
 - [3] W. G. Ellenbroek, E. Somfai, M. van Hecke, and W. van Saarloos, Phys. Rev. Lett. **97**, 258001 (2006).
 - [4] L. E. Silbert, A. J. Liu, and S. R. Nagel, Phys. Rev. E **79**, 021308 (2009).
 - [5] M. Wyart, S. R. Nagel, and T. A. Witten, EPL **72**, 486 (2005).
 - [6] M. Wyart, L. E. Silbert, S. R. Nagel, and T. A. Witten, Phys. Rev. E **72**, 051306 (2005).
 - [7] M. Wyart, EPL (Europhysics Letters) **89**, 64001 (2010).
 - [8] E. DeGiuli, A. Laversanne-Finot, G. During, E. Lerner, and M. Wyart, Soft Matter **10**, 5628 (2014).
 - [9] L. Yan, E. DeGiuli, and M. Wyart, EPL (Europhysics Letters) **114**, 26003 (2016).
 - [10] C. F. Schreck, N. Xu, and C. S. O’Hern, Soft Matter **6**, 2960 (2010).
 - [11] K. Shiraishi, H. Mizuno, and A. Ikeda, Phys. Rev. E **100**, 012606 (2019).
 - [12] K. Shiraishi, H. Mizuno, and A. Ikeda, Journal of the Physical Society of Japan **89**, 074603 (2020).
 - [13] L. E. Silbert, Phys. Rev. E **74**, 051303 (2006).
 - [14] C. P. Goodrich, A. J. Liu, and S. R. Nagel, Nature Phys. **10**, 578 (2014).
 - [15] H. Tong, P. Tan, and N. Xu, Scientific Reports **5**, 15378 (2015).
 - [16] P. Charbonneau, E. I. Corwin, L. Fu, G. Tsekenis, and M. van der Naald, Phys. Rev. E **99**, 020901 (2019).
 - [17] G. Tsekenis, arXiv:2006.07373 (2020).
 - [18] H. Ikeda, Phys. Rev. Research **2**, 033220 (2020).
 - [19] S. Franz, G. Parisi, P. Urbani, and F. Zamponi, Proceedings of the National Academy of Sciences **112**, 14539 (2015).
 - [20] P. J. Steinhardt, D. R. Nelson, and M. Ronchetti, Phys. Rev. B **28**, 784 (1983).
 - [21] A. Zaccone and E. Scossa-Romano,

- Phys. Rev. B **83**, 184205 (2011).
- [22] A. Zaccone, J. R. Blundell, and E. M. Terentjev, Phys. Rev. B **84**, 174119 (2011).
- [23] H. Mizuno, K. Saitoh, and L. E. Silbert, Phys. Rev. E **93**, 062905 (2016).
- [24] B. Cui, G. Ruocco, and A. Zaccone, Granular Matter **21**, 69 (2019).
- [25] C. F. Schreck, C. S. O'Hern, and L. E. Silbert, Physical Review E **84**, 011305 (2011).
- [26] L. E. Silbert, A. J. Liu, and S. R. Nagel, Phys. Rev. E **73**, 041304 (2006).
- [27] A. Lemaitre and C. Maloney, Journal of Statistical Physics **123**, 415 (2006).
- [28] H. Mizuno, S. Mossa, and J.-L. Barrat, EPL (Europhysics Letters) **104**, 56001 (2013).
- [29] E. Lerner, G. Düring, and E. Bouchbinder, Phys. Rev. Lett. **117**, 035501 (2016).
- [30] H. Mizuno, H. Shiba, and A. Ikeda, Proceedings of the National Academy of Sciences **114**, E97674 (2017).
- [31] L. Wang, A. Ninarello, P. Guan, L. Berthier, G. Szamel, and E. Flenner, Nature Communications **10**, 26 (2019).
- [32] H. Ikeda, Phys. Rev. E **99**, 050901 (2019).
- [33] M. Shimada, H. Mizuno, M. Wyart, and A. Ikeda, Phys. Rev. E **98**, 060901 (2018).
- [34] F. Leonforte, R. Boissière, A. Tanguy, J. P. Wittmer, and J.-L. Barrat, Phys. Rev. B **72**, 224206 (2005).
- [35] E. Lerner, E. DeGiuli, G. Düring, and M. Wyart, Soft Matter **10**, 5085 (2014).
- [36] K. Karimi and C. E. Maloney, Phys. Rev. E **92**, 022208 (2015).
- [37] G. Monaco and S. Mossa, Proc. Natl. Acad. Sci. USA **106**, 16907 (2009).
- [38] Y. M. Beltukov, C. Fusco, D. A. Parshin, and A. Tanguy, Phys. Rev. E **93**, 023006 (2016).
- [39] H. Mizuno and A. Ikeda, Phys. Rev. E **98**, 062612 (2018).
- [40] A. Moriel, G. Kapteijns, C. Rainone, J. Zylberg, E. Lerner, and E. Bouchbinder, The Journal of Chemical Physics **151**, 104503 (2019), <https://doi.org/10.1063/1.5111192>.
- [41] L. Wang, L. Berthier, E. Flenner, P. Guan, and G. Szamel, Soft Matter **15**, 7018 (2019).
- [42] K. Saitoh, R. K. Shrivastava, and S. Luding, Phys. Rev. E **99**, 012906 (2019).
- [43] N. Xu, V. Vitelli, A. J. Liu, and S. R. Nagel, EPL (Europhysics Letters) **90**, 56001 (2010).
- [44] H. Mizuno, M. Shimada, and A. Ikeda, Phys. Rev. Research **2**, 013215 (2020).
- [45] H. Mizuno, H. Tong, A. Ikeda, and S. Mossa, arXiv:2006.15082 (2020).
- [46] C. F. Schreck, T. Bertrand, C. S. O'Hern, and M. D. Shattuck, Phys. Rev. Lett. **107**, 078301 (2011).
- [47] S. van Deen, J. Simon, Z. Zeravcic, S. Dagois-Bohy, B. P. Tighe, and M. van Hecke, Phys. Rev. E **90**, 020202 (2014).
- [48] P. J. Tuckman, K. VanderWerf, Y. Yuan, S. Zhang, J. Zhang, M. D. Shattuck, and C. S. O'Hern, arXiv:2008.01895 (2020).
- [49] C. E. Maloney and A. Lemaitre, Phys. Rev. E **74**, 016118 (2006).
- [50] M. L. Manning and A. J. Liu, Phys. Rev. Lett. **107**, 108302 (2011).
- [51] R. Dasgupta, S. Karmakar, and I. Procaccia, Phys. Rev. Lett. **108**, 075701 (2012).
- [52] L. Gartner and E. Lerner, Phys. Rev. E **93**, 011001 (2016).
- [53] P. Morse, S. Wijtmans, M. van Deen, M. van Hecke, and M. L. Manning, Phys. Rev. Research **2**, 023179 (2020).